

---

# DIVER-0 : A Fully Channel Equivariant EEG Foundation Model

---

Danny Dongyeop Han<sup>\*1</sup> Ahhyun Lucy Lee<sup>\*2</sup> Taeyang Lee<sup>\*3</sup> Yonghyeon Gwon<sup>\*4</sup> Sebin Lee<sup>\*1</sup>  
Seong-jin Lee<sup>\*5</sup> David Keetae Park<sup>6</sup> Shinjae Yoo<sup>6</sup> Chun-kee Chung<sup>7,8</sup> Jiok Cha<sup>1,2,3</sup>

## Abstract

Electroencephalography (EEG) is a non-invasive technique widely used in brain-computer interfaces and clinical applications, yet existing EEG foundation models face limitations in modeling spatio-temporal brain dynamics and lack channel permutation equivariance, preventing robust generalization across diverse electrode configurations. To address these challenges, we propose DIVER-0, a novel EEG foundation model that demonstrates how full spatio-temporal attention—rather than segregated spatial or temporal processing—achieves superior performance when properly designed with Rotary Position Embedding (RoPE) for temporal relationships and binary attention biases for channel differentiation. We also introduce Sliding Temporal Conditional Positional Encoding (STCPE), which improves upon existing conditional positional encoding approaches by maintaining both temporal translation equivariance and channel permutation equivariance, enabling robust adaptation to arbitrary electrode configurations unseen during pretraining. Experimental results demonstrate that DIVER-0 achieves competitive performance with only 10% of pretraining data while maintaining consistent results across all channel permutation conditions, validating its effectiveness for cross-dataset generalization and establishing key design principles

for handling the inherent heterogeneity of neural recording setups.

## 1. Introduction

Electroencephalography (EEG) is a non-invasive neurophysiological technique that measures electrical activity generated by synchronized neuronal firing through electrodes placed on the scalp. With its high temporal resolution, portability, and affordability (Nicolas-Alonso & Gomez-Gil, 2012), EEG has been widely and effectively utilized in brain-computer interfaces (Schalk et al., 2004; Zhang et al., 2019), clinical diagnostics (Meghdadi et al., 2021), cognitive neuroscience research (Cohen, 2017), and in controlling assistive and rehabilitation devices for patients with neurological conditions (Meng et al., 2016).

EEG decoding has evolved significantly from early traditional machine learning approaches (Lotte et al., 2007) that relied on hand-crafted features to sophisticated deep learning architectures (Craik et al., 2019), including convolutional neural networks (Lawhern et al., 2018) and transformers (Song et al., 2022) that automatically learn hierarchical representations from raw signals (Schirrneister et al., 2017; Li et al., 2022; Bagchi & Bathula, 2022; Huang et al., 2022). More recently, following the success of foundation models in other domains, researchers have begun embracing self-supervised learning (SSL) paradigms, pre-training large-scale models on massive amounts of unlabeled EEG data (Wang et al., 2024a; Jiang et al., 2024; Mohammadi Foumani et al., 2024; Shi et al., 2024; Chien et al., 2022; Kostas et al., 2021; Wang et al., 2024b) to learn generic neural representations that can be fine-tuned for diverse downstream tasks. This paradigm shift promises to address fundamental challenges including data scarcity, cross-subject variability, and computational overhead of task-specific model development, while unlocking new capabilities for understanding and decoding complex neural signals.

However, existing EEG foundation models fail to address two critical limitations that constrain their effectiveness:

**Overly restrictive modeling of spatio-temporal brain dynamics.** Current approaches are constrained in its ability to

---

<sup>\*</sup>Equal contribution <sup>1</sup>Interdisciplinary Program of Artificial Intelligence, Seoul National University, Seoul, South Korea <sup>2</sup>Department of Brain and Cognitive Science, Seoul National University, Seoul, South Korea <sup>3</sup>Department of Psychology, Seoul National University, Seoul, South Korea <sup>4</sup>Interdisciplinary Program in Neuroscience, Seoul National University, Seoul, South Korea <sup>5</sup>Department of Medical Device Development, Seoul National University, Seoul, South Korea <sup>6</sup>Brookhaven National Laboratory, Upton, NY, USA <sup>7</sup>Department of Neurosurgery, Seoul National University Hospital, Seoul, South Korea <sup>8</sup>Department of Neurosurgery, Seoul National University Hospital, Seoul, South Korea. Correspondence to: Chun-kee Chung <chungc@snu.ac.kr>, Jiok Cha <connectome@snu.ac.kr>.

*Proceedings of the Workshop on Generative AI for Biology at the 42<sup>nd</sup> International Conference on Machine Learning*, Vancouver, Canada. PMLR 267, 2025. Copyright 2025 by the author(s).

capture the complex interactions between brain regions due to their treatment of multi-channel EEG data. Most methods fall into one of three restrictive categories. First, many approaches structurally segregate spatial and temporal processing by having separate spatial and temporal encoders (Chau et al., 2025; Zhang et al., 2023; Shi et al., 2024) or dedicated spatial and temporal attention blocks/heads (Dimofte et al., 2025; Wang et al., 2024b). While computationally efficient, this rigid separation cannot adequately model the brain’s distributed dynamics, where neural regions interact through temporally extended dependencies (Deco et al., 2011) and temporal and phase lags (Stam et al., 2007; Fries, 2005; Varela et al., 2001). Second, other methods collapse or flatten the channel dimension and eliminate spatial structure early in processing (Wang et al., 2024a; Mohammadi Foumani et al., 2024). This creates an information bottleneck that prevents the model from querying specific spatial relationships in later layers. Third, remaining approaches apply full attention with spatio-temporal input embeddings (Jiang et al., 2024), which means that they cannot adapt to electrodes not seen during pretraining, which is common in EEG where different researchers use varying electrode montages (Jurcak et al., 2007; Xu et al., 2020) or custom spatial configurations (Atcherson et al., 2007), limiting applicability across diverse recording setups.

**Lack of channel permutation equivariance and poor generalization across electrode configurations.** Current EEG foundation models fail to properly handle the fundamental requirement that model performance should be invariant to electrode ordering—a critical property for generalizing across diverse channel numbers and setups. Many methods use absolute channel embeddings that learn fixed representations for specific electrode positions, making them unable to generalize to unseen electrode configurations or montages. While recent methods like ACPE (Wang et al., 2024b) attempted to address cross-dataset transfer by using asymmetric conditional positional encoding to dynamically learn spatial relationships, it still fails to maintain proper permutation equivariance because it applies convolutions across both spatial (channel) and temporal dimensions simultaneously. This architectural choice breaks the fundamental mathematical property that the model should perform identically regardless of channel ordering.

To address these limitations, we propose a full-attention architecture with novel condition positional encoding schemes that maintain both temporal translation equivariance and channel permutation equivariance, enabling robust generalization across diverse electrode configurations and experimental setups.

- We present **DIVER-0**, a new EEG foundation model that demonstrates competitive performance across rep-

resentative downstream BCI tasks with different electrode configurations, while maintaining strict permutation equivariance—a critical property for cross-dataset generalization.

- We introduce the **DIVER transformer block** with unified spatio-temporal attention, combining Rotary Position Embedding (RoPE) (Su et al., 2024) for temporal relationships and binary attention biases (Woo et al., 2024) for channel differentiation while maintaining permutation equivariance across electrode orderings.
- We propose **Sliding Temporal Conditional Positional Encoding (STCPE)** that preserves both temporal translation equivariance and channel permutation equivariance, enabling robust generalization to arbitrary electrode configurations unseen during pretraining.

## 2. Methods

### 2.1. Architecture

#### 2.1.1. PATCH ENCODING

We divide the raw EEG signal from each channel into small patches of 1 second duration, with each patch containing 200 samples (at 200 Hz sampling rate). After masking, each patch undergoes a two-step patch encoding process. First, the raw patch is processed through patch-wise convolutional neural networks (CNNs) to extract temporal features. The spectral pathway then applies Fast Fourier Transform (FFT) to this CNN output. The final patch encoding is obtained by element-wise addition of the CNN features and their frequency domain transformation. This approach creates a unified patch representation that combines the original temporal features with their spectral characteristics derived from the same CNN-processed signal.

#### 2.1.2. SLIDING TEMPORAL CONDITIONAL POSITIONAL EMBEDDING (STCPE)

Following patch encoding, we apply Sliding Temporal Conditional Positional Embedding (STCPE). Conditional Positional Encoding (CPE) originally uses convolutional networks to dynamically generate positional encodings from spatial-temporal neighborhoods, which was successfully adapted as Asymmetric Conditional Positional Encoding (ACPE) in CBraMod (Wang et al., 2024b), achieving state-of-the-art performance across multiple downstream BCI tasks. The STCPE mechanism, in contrast, operates by sliding a transformer block across the temporal dimension, where at each time step, the transformer processes patches from *all channels simultaneously*, computing positional information by aggregating outputs across this temporal sliding window. The STCPE is constructed using DIVER encoder blocks (see Section 2.1.3), which incorporate both

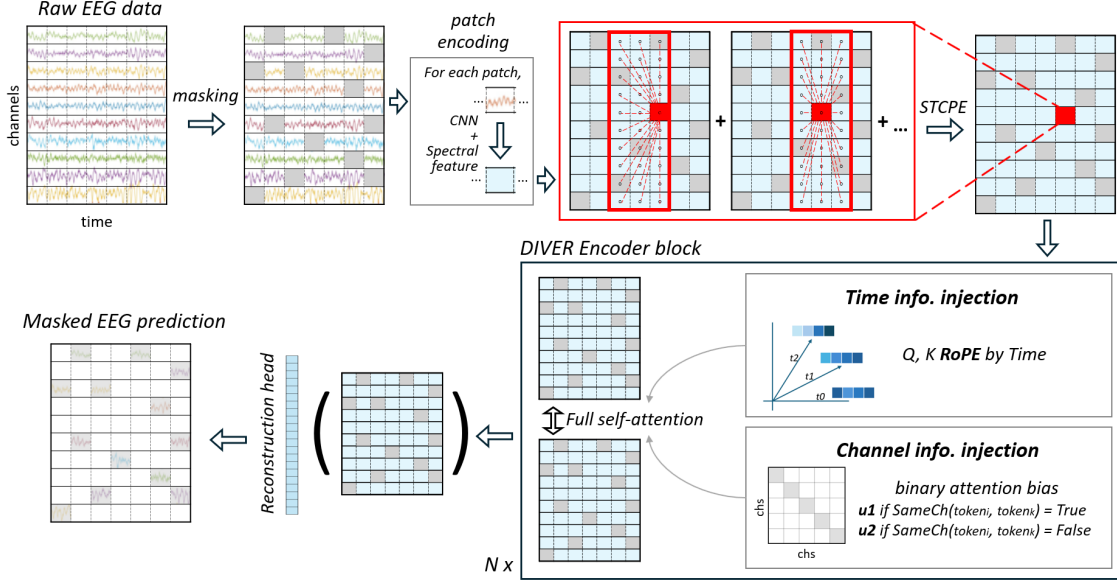


**Figure 1. Overview of DIVER-0 architecture and pretraining** EEG signals are segmented into 1-second patches (200 samples at 200 Hz). After masking, each patch undergoes patch encoding through patch-wise convolutional neural networks (CNNs) for temporal features, with spectral features obtained via Fast Fourier Transform (FFT) and element-wise addition. The Sliding Temporal Conditional Positional Embedding (STCPE) is computed by summing outputs from sliding transformer encoders across the temporal dimension. These embeddings are then processed by DIVER encoder blocks, which employ unified full self-attention across both temporal and spatial dimensions. Within each encoder block, temporal relationships are encoded using Rotary Position Embedding (RoPE) (Su et al., 2024), while channel identity is encoded through binary attention biases (Woo et al., 2024; Liu et al., 2024). The model is pretrained using masked patch reconstruction.

Rotary Position Embedding (RoPE) (Su et al., 2024) for temporal awareness and binary attention bias (Woo et al., 2024) for channel differentiation, enabling the model to distinguish between different channels and timepoints during the positional encoding process.

Unlike ACPE (Wang et al., 2024b) that applies asymmetric convolutions across both spatial (channel) and temporal dimensions simultaneously, our STCPE design maintains crucial mathematical properties: **temporal translation equivariance** and **channel-wise permutation equivariance**. This enables STCPE to provide generalizable positional encodings for arbitrary electrode orderings and configurations not seen during pretraining, while also being invariant to temporal shifts in the input signals.

To manage computational complexity, linear projection layers are applied before and after STCPE to reduce the embedding dimension during this positional encoding stage. The final patch embeddings with positional information are obtained as  $\mathbf{X}^o = \mathbf{X} + \mathbf{PE} = \{\mathbf{x}_{i,j} + \mathbf{pe}_{i,j} | i \in [1, 2, \dots, C], j \in [1, 2, \dots, N]\}$ , where  $\mathbf{X}^o \in \mathbb{R}^{C \times N \times D}$  represents the patch embeddings enhanced with relative positional information.

### 2.1.3. DIVER ENCODER

After applying the STCPE, the sequence of embeddings is fed into the DIVER encoder, which follows a structure similar to the full attention Transformer enhanced with components from MOIRAI (Woo et al., 2024). The encoder incorporates two key mechanisms: rotary positional embedding to encode temporal relationships between time points, and binary attention bias to inform the model when two electrodes represent the same channel.

The attention mechanism can be formulated as follows, where for clarity we omit layer and attention head indices as well as scaling factors. The attention score between the  $(i, m)$ -th query (where  $i$  denotes the time index and  $m$  denotes the electrode index) and the  $(j, n)$ -th key is computed as:

$$E_{ij,mn} = (\mathbf{W}^Q \mathbf{x}_{i,m})^T \mathbf{R}_{i-j} (\mathbf{W}^K \mathbf{x}_{j,n}) + u^1 * \mathbb{1}_{\{m=n\}} + u^2 * \mathbb{1}_{\{m \neq n\}}, \quad (1)$$

$$A_{ij,mn} = \frac{\exp\{E_{ij,mn}\}}{\sum_{k,o} \exp\{E_{ik,mo}\}}$$

where  $\mathbf{W}^Q \mathbf{x}_{i,m}, \mathbf{W}^K \mathbf{x}_{j,n} \in \mathbb{R}^{d_h}$  are the query and key vectors,  $\mathbf{R}_{i-j} \in \mathbb{R}^{d_h \times d_h}$  is the rotary projection matrix,  $u^1, u^2 \in \mathbb{R}$  are learnable scalars that can be different in

each head,  $\mathbb{1}_{\{cond\}} = 1$  if *cond* is true, and  $\mathbb{1}_{\{cond\}} = 0$  otherwise.

## 2.2. Pretraining

DIVER was pretrained on the extensive Temple University Hospital EEG Corpus (TUEG) dataset (Obeid & Picone, 2016), one of the largest publicly available EEG datasets comprising of 69,652 clinical recordings from 14,987 subjects. This dataset provides approximately 30,000 hours of EEG data, ideal for pretraining models to learn robust neural representations across diverse clinical populations and pathological conditions.

The preprocessing pipeline closely followed the methodology established in CBraMod (Wang et al., 2024b). Briefly, the raw EEG signals underwent bandpass filtering (0.3-75 Hz) to remove low and high-frequency artifacts, followed by a 60 Hz notch filter to eliminate power line interference. All recordings were resampled to 200 Hz and segmented into 30-second non-overlapping training samples. Signals exceeding 100  $\mu$ V amplitude were automatically rejected to ensure data quality, and 19 standard EEG channels following the 10-20 system were selected for analysis.

The DIVER backbone consists of 12 DIVER encoder blocks with a hidden dimension of 200, inner feed-forward dimensions of 800, and 10 attention heads. As illustrated in Figure 1, the model also employs a novel embedding strategy combining patch-wise CNN projection, spectral features, and Sliding Temporal Conditional Positional Encoding (STCPE) with a temporal window size of 7 seconds.

Training was conducted using the AdamW optimizer with a learning rate of  $5 \times 10^{-4}$  for pretraining on 10% of the data and  $1 \times 10^{-4}$  for full dataset pretraining, with corresponding weight decay values of  $5 \times 10^{-4}$  and  $1 \times 10^{-3}$  respectively. The model was implemented using Python 3.12.7 and PyTorch 2.5.1 with CUDA 12.1 support, and training was performed on compute nodes equipped with four NVIDIA A100 40GB GPUs.

## 2.3. Finetuning

Finetuning was done on two downstream datasets, FACED and PhysioNet-MI. FACED dataset (Chen et al., 2023) contains 32-channel EEG recordings from 123 subjects who watched 28 emotion-elicitation video clips covering nine emotion categories. PhysioNet-MI (Goldberger et al., 2000) refers to the EEG Motor Movement/Imagery Dataset from PhysioNet (Goldberger et al., 2000), which consists of more than 1500 EEG recordings from 109 volunteers performing a series of real and imagined motor tasks, with data recorded from 64 electrodes. Implementation details including hyperparameters are detailed in Appendix A.1.

# 3. Experiments

## 3.1. Downstream Task Performance

We evaluate DIVER-0 on two representative BCI tasks, FACED (Chen et al., 2023) and PhysioNet-MI (Goldberger et al., 2000), with different electrode configurations. Table 1 presents the performance comparison against state-of-the-art baselines including both non-foundation models (EEGNet, SPaRCNet, ST-Transformer, EEGConformer) and recent EEG foundation models (LaBraM-Base, CBraMod).

DIVER-0 pretrained on 10% of the TUEG corpus achieves competitive performance across both tasks. On FACED, DIVER-0 achieves 59.2% balanced accuracy and 54.0% Cohen’s Kappa, outperforming all baselines including CBraMod (55.1% balanced accuracy). On PhysioNet-MI, DIVER-0 achieves 62.8% balanced accuracy and 50.4% Cohen’s Kappa, demonstrating robust cross-dataset transfer. While CBraMod achieves slightly higher performance (64.2%), DIVER-0’s competitive results using only 10% of pretraining data highlight the efficiency of our approach.

These results validate the effectiveness of our unified spatio-temporal attention approach and STCPE for handling diverse electrode configurations while maintaining strict permutation equivariance.

## 3.2. Component Ablation Analysis

To validate the contribution of each architectural component, we conduct comprehensive ablation studies presented in Table 2. For computational efficiency, all models in this analysis were pretrained using 10% of the TUEG corpus. We systematically remove or replace key components: patch-wise CNN encoding, spectral embedding, STCPE, RoPE, binary attention biases, and compare different transformer block designs.

The results reveal nuanced insights about component contributions across different task types. On the FACED emotion recognition task, DIVER-0 achieves the highest performance (59.2% balanced accuracy), with each component contributing meaningfully: removing patch-wise CNN encoding leads to a 1.9% drop, removing spectral embedding causes a 1.2% decrease, and replacing DIVER blocks with vanilla transformers results in a substantial 3.9% performance degradation. This validates the effectiveness of our unified spatio-temporal attention for complex, distributed brain processes involved in emotion recognition.

Interestingly, on the PhysioNet-MI motor imagery task, while DIVER-0 outperforms CBraMod 10% (62.8% vs 62.4%), some ablated configurations achieve slightly higher performance. Specifically, removing spectral embedding yields 63.4% balanced accuracy, and replacing DIVER blocks with CBraMod blocks achieves 63.1%.



**Table 1. Performance comparison on downstream EEG tasks.** Results are reported for emotion recognition (FACED, 9-class) and motor imagery classification (PhysioNet-MI, 4-class). Performance values for baseline methods are quoted from (Wang et al., 2024b) using identical preprocessing and evaluation protocols. DIVER results are from our experiments. All metrics are reported as mean  $\pm$  standard deviation across 5 random seeds. DIVER 10% indicate that the model was pretrained using 10% of the full TUEG dataset.

Methods	FACED, 9-class			PhysioNet-MI, 4-class		
	Bal. Acc.(%)	Kappa (%)	F1(%)	Bal. Acc. (%)	Kappa(%)	F1(%)
EEGNet	40.9 $\pm$ 1.2	33.4 $\pm$ 2.5	41.2 $\pm$ 1.4	58.1 $\pm$ 1.3	44.7 $\pm$ 2.0	58.0 $\pm$ 1.2
SPaRCNet	46.7 $\pm$ 1.6	39.8 $\pm$ 2.9	47.3 $\pm$ 1.3	59.3 $\pm$ 1.5	45.6 $\pm$ 2.3	59.4 $\pm$ 1.5
ST-Transformer	48.1 $\pm$ 0.8	41.4 $\pm$ 1.3	48.0 $\pm$ 1.0	60.4 $\pm$ 0.8	47.1 $\pm$ 2.0	60.5 $\pm$ 0.8
EEGConformer	45.6 $\pm$ 1.3	38.6 $\pm$ 1.9	45.1 $\pm$ 1.1	60.5 $\pm$ 1.0	47.4 $\pm$ 1.7	60.6 $\pm$ 1.0
LaBraM-Base	52.7 $\pm$ 1.1	47.0 $\pm$ 1.9	52.9 $\pm$ 1.0	61.7 $\pm$ 1.2	49.1 $\pm$ 1.9	61.8 $\pm$ 1.4
CBraMod	55.1 $\pm$ 0.9	50.4 $\pm$ 1.2	56.2 $\pm$ 0.9	<b>64.2 <math>\pm</math> 0.9</b>	<b>52.2 <math>\pm</math> 1.7</b>	<b>64.3 <math>\pm</math> 1.0</b>
<b>DIVER 10% (Ours)</b>	<b>59.2 <math>\pm</math> 0.8</b>	<b>54.0 <math>\pm</math> 0.9</b>	<b>59.6 <math>\pm</math> 0.7</b>	62.8 $\pm$ 0.5	50.4 $\pm$ 0.7	62.9 $\pm$ 0.5

**Table 2. Ablation analysis of pretrained model components.** Results are reported for emotion recognition (FACED, 9-class) and motor imagery classification (PhysioNet-MI, 4-class). DIVER 10% and CBraMod 10% indicate that the models were pretrained using 10% of the full TUEG dataset. All metrics are reported as mean  $\pm$  standard deviation across 5 random seeds.

Methods	FACED, 9-class			PhysioNet-MI, 4-class		
	Bal. Acc. (%)	Kappa(%)	F1(%)	Bal. Acc. (%)	Kappa(%)	F1(%)
<b>DIVER 10% (Ours)</b>	<b>59.2 <math>\pm</math> 0.8</b>	<b>54.0 <math>\pm</math> 0.9</b>	<b>59.6 <math>\pm</math> 0.7</b>	62.8 $\pm$ 0.5	50.4 $\pm$ 0.7	62.9 $\pm$ 0.5
w/o patch-wise CNN encoding	57.3 $\pm$ 0.9	51.7 $\pm$ 1.0	57.4 $\pm$ 0.9	61.9 $\pm$ 0.5	49.3 $\pm$ 0.6	62.1 $\pm$ 0.5
w/o spectral embedding	58.0 $\pm$ 1.1	52.6 $\pm$ 1.3	58.3 $\pm$ 1.2	<b>63.4 <math>\pm</math> 0.5</b>	<b>51.1 <math>\pm</math> 0.6</b>	<b>63.5 <math>\pm</math> 0.5</b>
w/o STCPE	58.4 $\pm$ 1.0	53.0 $\pm$ 1.1	58.6 $\pm$ 1.0	62.8 $\pm$ 0.5	50.5 $\pm$ 0.6	63.0 $\pm$ 0.5
STCPE $\rightarrow$ ACPE	58.7 $\pm$ 0.9	53.4 $\pm$ 1.1	59.0 $\pm$ 1.0	62.4 $\pm$ 0.3	49.9 $\pm$ 0.4	62.5 $\pm$ 0.3
w/o RoPE	57.7 $\pm$ 0.6	52.2 $\pm$ 0.7	58.1 $\pm$ 0.6	62.6 $\pm$ 0.4	50.2 $\pm$ 0.5	62.8 $\pm$ 0.4
w/o Binary attention bias	58.1 $\pm$ 1.0	52.6 $\pm$ 1.1	58.4 $\pm$ 1.0	62.8 $\pm$ 0.5	50.4 $\pm$ 0.7	63.0 $\pm$ 0.6
DIVER $\rightarrow$ Vanilla block	55.3 $\pm$ 1.9	49.5 $\pm$ 2.2	55.5 $\pm$ 1.9	61.6 $\pm$ 1.5	48.8 $\pm$ 1.9	61.7 $\pm$ 1.5
DIVER $\rightarrow$ CBraMod block	57.0 $\pm$ 0.6	51.5 $\pm$ 0.6	57.4 $\pm$ 0.5	63.1 $\pm$ 0.8	50.8 $\pm$ 1.0	63.2 $\pm$ 0.8
CBraMod 10%	56.5 $\pm$ 0.8	51.0 $\pm$ 1.0	56.9 $\pm$ 0.8	62.4 $\pm$ 0.6	49.9 $\pm$ 0.8	62.6 $\pm$ 0.7

This pattern suggests that motor imagery classification, which involves localized cortical sources around the sensorimotor cortex (Hameed et al., 2025; Smith et al., 2014), may benefit from more constrained attention patterns that focus on specific spatial-temporal relationships rather than full spatio-temporal interactions. This contrasts with emotion processing, which involves distributed cortico-limbic circuits encompassing deep subcortical structures such as the amygdala, hippocampus, and anterior insula (Pessoa, 2017), whose widespread cortical manifestations in EEG activity benefit from our model’s ability to capture long-range spatio-temporal dependencies (Liu et al., 2023; Valderrama & Sheoran, 2025). In fact, motor imagery BCI is primarily confined to accessible sensorimotor cortical areas (Kim et al., 2025), where more focused attention mechanisms may be sufficient. The relatively small dataset size of PhysioNet-MI may also favor the reduced parameter complexity of ablated configurations over the full model’s capacity to capture complex distributed interactions.

These results highlight an important insight: while unified spatio-temporal attention excels for distributed brain

processes (emotion recognition), more focused attention mechanisms may be advantageous for spatially localized tasks (motor imagery), particularly with limited training data. Nevertheless, DIVER-0 demonstrates competitive performance across both task types while maintaining the crucial advantage of permutation equivariance for cross-dataset generalization.

### 3.3. Channel Permutation Analysis

A key advantage of DIVER-0 is its permutation equivariance with respect to channel ordering. Table 3 presents a systematic analysis where we evaluate models under four conditions: intact pretraining with intact finetuning, intact pretraining with permuted finetuning, permuted pretraining with intact finetuning, and permuted pretraining with permuted finetuning. To isolate the encoder’s robustness, our permutation protocol involves permuting the input channels, processing them through the encoder, then permuting them back to the original order before the classifier, ensuring we specifically test the underlying model’s channel permutation robustness rather than classifier adaptation.

Table 3. Performance comparison across Pretraining  $\times$  Finetuning configurations on the FACED dataset. Balanced Accuracy, Kappa, and F1 are reported. ('w/o' denotes our model without the corresponding component, and ' $\rightarrow$ ' denotes replacement of our model's component with the alternative component.)

		Pretrain						
		Intact			Permute			
Finetuning	Methods	Bal. Acc.(%)	Kappa(%)	F1(%)	Bal. Acc.(%)	Kappa(%)	F1(%)	
	Intact	DIVER 10% (Ours)	59.2 ± 0.9	54.0 ± 0.9	59.6 ± 0.7	59.6 ± 0.8	54.4 ± 0.9	59.9 ± 0.8
		w/o STCPE	58.4 ± 1.0	53.0 ± 1.1	58.6 ± 1.0	58.4 ± 0.8	52.9 ± 0.9	58.5 ± 0.8
		STCPE → ACPE	56.7 ± 1.1	51.2 ± 1.3	57.2 ± 1.1	60.1 ± 0.9	54.8 ± 1.1	60.3 ± 0.9
		w/o Binary attention bias	58.1 ± 1.0	52.6 ± 1.1	58.4 ± 1.0	58.1 ± 1.3	52.7 ± 1.4	58.5 ± 1.2
		DIVER → Vanilla block	55.3 ± 1.9	49.5 ± 2.2	55.5 ± 1.9	56.3 ± 0.7	50.7 ± 0.9	56.6 ± 0.8
		DIVER → CBraMod block	57.0 ± 0.6	51.5 ± 0.6	57.4 ± 0.5	56.8 ± 0.6	51.2 ± 0.7	57.1 ± 0.6
		CBraMod 10%	56.5 ± 0.8	51.0 ± 1.0	56.9 ± 0.8	58.7 ± 0.4	53.4 ± 0.4	59.0 ± 0.5
	Permute	DIVER 10% (Ours)	59.1 ± 0.4	53.8 ± 0.5	59.4 ± 0.3	59.0 ± 0.7	53.6 ± 0.8	59.3 ± 0.7
		w/o STCPE	58.7 ± 0.4	53.3 ± 0.4	58.9 ± 0.3	59.1 ± 0.4	53.6 ± 0.4	58.9 ± 0.2
		STCPE → ACPE	60.1 ± 0.9	54.8 ± 1.0	60.3 ± 0.8	58.8 ± 0.4	53.4 ± 0.5	59.1 ± 0.4
		w/o Binary attention bias	58.6 ± 1.2	53.2 ± 1.4	58.9 ± 1.3	58.7 ± 0.2	53.3 ± 0.2	59.0 ± 0.2
		DIVER → Vanilla block	57.6 ± 1.7	51.8 ± 1.8	57.9 ± 0.2	55.6 ± 0.8	49.9 ± 0.9	55.9 ± 0.7
		DIVER → CBraMod block	57.0 ± 0.8	51.4 ± 0.9	57.3 ± 0.9	57.1 ± 0.6	51.6 ± 0.7	57.4 ± 0.6
CBraMod 10%		56.5 ± 0.5	50.9 ± 0.6	56.8 ± 0.5	58.0 ± 0.9	52.5 ± 1.1	58.2 ± 1.0	

DIVER-0 demonstrates remarkable robustness across all permutation conditions, with balanced accuracy remaining virtually unchanged (ranging from 59.0% to 59.6%) regardless of channel ordering during pretraining or finetuning. This stability validates our claim about permutation equivariance and demonstrates practical advantages for real-world deployment where electrode montages may vary across research groups and clinical settings.

Interestingly, when STCPE is replaced with ACPE, we observe a nuanced pattern: ACPE performs well when either pretraining or finetuning involves permutation, but shows degraded performance when both are intact or both are permuted. We hypothesize this occurs because ACPE's convolutional design can adapt to become agnostic to channel orderings during permuted pretraining, learning spatially-invariant representations. Subsequently, during intact finetuning, ACPE can leverage its inherent channel discrimination capabilities to exploit specific spatial relationships.

This analysis reveals an important trade-off: while our current STCPE achieves robust permutation equivariance through binary channel differentiation (distinguishing same-channel from cross-channel interactions), it sacrifices detailed channel-specific discrimination (the ability to identify and leverage individual electrode characteristics). Future work could explore injecting explicit channel position information alongside binary attention biases to maintain permutation equivariance while enabling finer-grained spatial awareness. Nevertheless, DIVER-0's consistent performance across all permutation conditions demonstrates

the practical value of our approach for robust cross-dataset generalization.

## 4. Conclusion

We present DIVER-0, a novel EEG foundation model that addresses critical limitations in existing approaches through two key innovations. First, we introduce the DIVER transformer block with unified spatio-temporal attention, combining Rotary Position Embedding (RoPE) for temporal relationships and binary attention biases for channel differentiation. Second, we propose Sliding Temporal Conditional Positional Encoding (STCPE), which maintains both temporal translation equivariance and channel permutation equivariance.

Our experiments demonstrate that DIVER-0 achieves competitive performance across representative BCI tasks while maintaining strict permutation equivariance, enabling robust generalization to unseen electrode configurations. Notably, even when pretrained on only 10% of the TUEG corpus, DIVER-0 outperforms existing foundation models on emotion recognition tasks, highlighting the effectiveness of our unified spatio-temporal attention approach for distributed brain processes.

Furthermore, the consistent performance of DIVER-0 across all channel permutation conditions demonstrates the practical value of maintaining strict permutation equivariance for cross-dataset generalization. Our unified spatio-temporal attention approach successfully captures complex neural

dynamics while preserving the mathematical properties essential for robust deployment across diverse electrode configurations.

**Future Work.** Several directions warrant investigation: (1) Rigorous evaluation across more diverse datasets and tasks to systematically validate our hypothesis that unified spatio-temporal attention benefits tasks involving distributed brain networks (e.g., emotion, cognition) while spatially constrained attention may be more suitable for localized cortical processes (e.g., sensorimotor functions); (2) Developing methods to incorporate explicit channel position information while maintaining permutation equivariance, potentially through relative biases or unified topology mapping approaches as explored in MMM (Yi et al., 2023); (3) Scaling to larger datasets (full TUEG and additional EEG corpora) and model sizes to explore the limits of EEG foundation model capabilities; (4) Systematic analysis of why ACPE combined with channel permutation shows promising results in certain conditions, and whether this transfers to other downstream applications.

Our work demonstrates the importance of inherently modeling both spatial and temporal EEG dynamics through unified attention mechanisms with embedded channel differentiation via binary attention biases. The success of full spatio-temporal attention for distributed brain processes, combined with the critical requirement for permutation equivariance, establishes key design principles for future EEG foundation models. DIVER-0 thus provides a robust foundation for handling the inherent heterogeneity of neural recording setups while maintaining mathematical guarantees essential for cross-dataset generalization.

## Acknowledgements

This research used resources of the Oak Ridge Leadership Computing Facility, which is a DOE Office of Science User Facility supported under Contract DE-AC05-00OR22725.

## Impact Statement

This paper presents work whose goal is to advance the field of Machine Learning and neuroscience. There are many potential societal consequences of our work, none which we feel must be specifically highlighted here.

## References

Atcherson, S. R., Gould, H. J., Pousson, M. A., and Prout, T. M. Variability of electrode positions using electrode caps. *Brain topography*, 20:105–111, 2007.

Bagchi, S. and Bathula, D. R. Eeg-convtransformer for single-trial eeg-based visual stimulus classification. *Pat-*

*tern Recognition*, 129:108757, 2022.

Chau, G., Wang, C., Talukder, S., Subramaniam, V., Soedar-madji, S., Yue, Y., Katz, B., and Barbu, A. Population transformer: Learning population-level representations of neural activity. *ArXiv*, pp. arXiv-2406, 2025.

Chen, J., Wang, X., Huang, C., Hu, X., Shen, X., and Zhang, D. A large finer-grained affective computing eeg dataset. *Scientific Data*, 10(1):740, 2023.

Chien, H.-Y. S., Goh, H., Sandino, C. M., and Cheng, J. Y. Maeeg: Masked auto-encoder for eeg representation learning. *arXiv preprint arXiv:2211.02625*, 2022.

Cohen, M. X. Where does eeg come from and what does it mean? *Trends in neurosciences*, 40(4):208–218, 2017.

Craik, A., He, Y., and Contreras-Vidal, J. L. Deep learning for electroencephalogram (eeg) classification tasks: a review. *Journal of neural engineering*, 16(3):031001, 2019.

Deco, G., Jirsa, V. K., and McIntosh, A. R. Emerging concepts for the dynamical organization of resting-state activity in the brain. *Nature reviews neuroscience*, 12(1): 43–56, 2011.

Dimofte, A., Bucagu, G. A., Ingolfsson, T. M., Wang, X., Cossetini, A., Benini, L., and Li, Y. Cerebro: Compact encoder for representations of brain oscillations using efficient alternating attention. *arXiv preprint arXiv:2501.10885*, 2025.

Fries, P. A mechanism for cognitive dynamics: neuronal communication through neuronal coherence. *Trends in cognitive sciences*, 9(10):474–480, 2005.

Goldberger, A. L., Amaral, L. A., Glass, L., Hausdorff, J. M., Ivanov, P. C., Mark, R. G., Mietus, J. E., Moody, G. B., Peng, C.-K., and Stanley, H. E. Physiobank, physiotoolkit, and physionet: components of a new research resource for complex physiologic signals. *circulation*, 101(23): e215–e220, 2000.

Hameed, I., Khan, D. M., Ahmed, S. M., Aftab, S. S., and Fazal, H. Enhancing motor imagery eeg signal decoding through machine learning: A systematic review of recent progress. *Computers in Biology and Medicine*, 185:109534, 2025.

Huang, W., Chang, W., Yan, G., Yang, Z., Luo, H., and Pei, H. Eeg-based motor imagery classification using convolutional neural networks with local reparameterization trick. *Expert Systems with Applications*, 187:115968, 2022.

Jiang, W.-B., Zhao, L.-M., and Lu, B.-L. Large brain model for learning generic representations with tremendous eeg data in bci. *arXiv preprint arXiv:2405.18765*, 2024.

- Jurcak, V., Tsuzuki, D., and Dan, I. 10/20, 10/10, and 10/5 systems revisited: their validity as relative head-surface-based positioning systems. *Neuroimage*, 34(4): 1600–1611, 2007.
- Kim, S.-H., Kim, S.-J., and Lee, D.-H. Neurophysiological analysis in motor and sensory cortices for improving motor imagination. In *2025 13th International Conference on Brain-Computer Interface (BCI)*, pp. 1–4. IEEE, 2025.
- Kostas, D., Aroca-Ouellette, S., and Rudzicz, F. Bendr: Using transformers and a contrastive self-supervised learning task to learn from massive amounts of eeg data. *Frontiers in Human Neuroscience*, 15:653659, 2021.
- Langley, P. Crafting papers on machine learning. In Langley, P. (ed.), *Proceedings of the 17th International Conference on Machine Learning (ICML 2000)*, pp. 1207–1216, Stanford, CA, 2000. Morgan Kaufmann.
- Lawhern, V. J., Solon, A. J., Waytowich, N. R., Gordon, S. M., Hung, C. P., and Lance, B. J. Eegnet: a compact convolutional neural network for eeg-based brain-computer interfaces. *Journal of neural engineering*, 15(5):056013, 2018.
- Li, H., Ding, M., Zhang, R., and Xiu, C. Motor imagery eeg classification algorithm based on cnn-lstm feature fusion network. *Biomedical signal processing and control*, 72: 103342, 2022.
- Liu, J., Hu, X., Shen, X., Lv, Z., Song, S., and Zhang, D. The eeg microstate representation of discrete emotions. *International Journal of Psychophysiology*, 186:33–41, 2023.
- Liu, X., Liu, J., Woo, G., Aksu, T., Liang, Y., Zimmermann, R., Liu, C., Savarese, S., Xiong, C., and Sahoo, D. Moirai-moe: Empowering time series foundation models with sparse mixture of experts. *arXiv preprint arXiv:2410.10469*, 2024.
- Lotte, F., Congedo, M., Lécuyer, A., Lamarche, F., and Arnaldi, B. A review of classification algorithms for eeg-based brain-computer interfaces. *Journal of neural engineering*, 4(2):R1, 2007.
- Meghdadi, A. H., Stevanović Karić, M., McConnell, M., Rupp, G., Richard, C., Hamilton, J., Salat, D., and Berka, C. Resting state eeg biomarkers of cognitive decline associated with alzheimer’s disease and mild cognitive impairment. *PloS one*, 16(2):e0244180, 2021.
- Meng, J., Zhang, S., Bekyo, A., Olsoe, J., Baxter, B., and He, B. Noninvasive electroencephalogram based control of a robotic arm for reach and grasp tasks. *Scientific Reports*, 6(1):38565, 2016.
- Mohammadi Foumani, N., Mackellar, G., Ghane, S., Irtza, S., Nguyen, N., and Salehi, M. Eeg2rep: enhancing self-supervised eeg representation through informative masked inputs. In *Proceedings of the 30th ACM SIGKDD Conference on Knowledge Discovery and Data Mining*, pp. 5544–5555, 2024.
- Nicolas-Alonso, L. F. and Gomez-Gil, J. Brain computer interfaces, a review. *sensors*, 12(2):1211–1279, 2012.
- Obeid, I. and Picone, J. The temple university hospital eeg data corpus. *Frontiers in neuroscience*, 10:196, 2016.
- Pessoa, L. A network model of the emotional brain. *Trends in cognitive sciences*, 21(5):357–371, 2017.
- Schalk, G., McFarland, D. J., Hinterberger, T., Birbaumer, N., and Wolpaw, J. R. Bci2000: a general-purpose brain-computer interface (bci) system. *IEEE Transactions on biomedical engineering*, 51(6):1034–1043, 2004.
- Schirrneister, R. T., Springenberg, J. T., Fiederer, L. D. J., Glasstetter, M., Eggersperger, K., Tangermann, M., Hutter, F., Burgard, W., and Ball, T. Deep learning with convolutional neural networks for eeg decoding and visualization. *Human brain mapping*, 38(11):5391–5420, 2017.
- Shi, E., Zhao, K., Yuan, Q., Wang, J., Hu, H., Yu, S., and Zhang, S. Fome: A foundation model for eeg using adaptive temporal-lateral attention scaling. *arXiv preprint arXiv:2409.12454*, 2024.
- Smith, M. M., Weaver, K. E., Grabowski, T. J., Rao, R. P., and Darvas, F. Non-invasive detection of high gamma band activity during motor imagery. *Frontiers in human neuroscience*, 8:817, 2014.
- Song, Y., Zheng, Q., Liu, B., and Gao, X. Eeg conformer: Convolutional transformer for eeg decoding and visualization. *IEEE Transactions on Neural Systems and Rehabilitation Engineering*, 31:710–719, 2022.
- Stam, C. J., Nolte, G., and Daffertshofer, A. Phase lag index: assessment of functional connectivity from multi channel eeg and meg with diminished bias from common sources. *Human brain mapping*, 28(11):1178–1193, 2007.
- Su, J., Ahmed, M., Lu, Y., Pan, S., Bo, W., and Liu, Y. Roformer: Enhanced transformer with rotary position embedding. *Neurocomputing*, 568:127063, 2024.
- Valderrama, C. E. and Sheoran, A. Identifying relevant eeg channels for subject-independent emotion recognition using attention network layers. *Frontiers in Psychiatry*, 16:1494369, 2025.



- Varela, F., Lachaux, J.-P., Rodriguez, E., and Martinerie, J. The brainweb: phase synchronization and large-scale integration. *Nature reviews neuroscience*, 2(4):229–239, 2001.
- Wang, G., Liu, W., He, Y., Xu, C., Ma, L., and Li, H. Eegpt: Pretrained transformer for universal and reliable representation of eeg signals. *Advances in Neural Information Processing Systems*, 37:39249–39280, 2024a.
- Wang, J., Zhao, S., Luo, Z., Zhou, Y., Jiang, H., Li, S., Li, T., and Pan, G. Cbramod: A criss-cross brain foundation model for eeg decoding. *arXiv preprint arXiv:2412.07236*, 2024b.
- Woo, G., Liu, C., Kumar, A., Xiong, C., Savarese, S., and Sahoo, D. Unified training of universal time series forecasting transformers. *International Conference on Machine Learning*, 2024.
- Xu, L., Xu, M., Ke, Y., An, X., Liu, S., and Ming, D. Cross-dataset variability problem in eeg decoding with deep learning. *Frontiers in human neuroscience*, 14:103, 2020.
- Yi, K., Wang, Y., Ren, K., and Li, D. Learning topology-agnostic eeg representations with geometry-aware modeling. *Advances in Neural Information Processing Systems*, 36:53875–53891, 2023.
- Zhang, D., Yuan, Z., Yang, Y., Chen, J., Wang, J., and Li, Y. Brant: Foundation model for intracranial neural signal. *Advances in Neural Information Processing Systems*, 36: 26304–26321, 2023.
- Zhang, S., Yuan, S., Huang, L., Zheng, X., Wu, Z., Xu, K., and Pan, G. Human mind control of rat cyborg’s continuous locomotion with wireless brain-to-brain interface. *Scientific reports*, 9(1):1321, 2019.

## A. Implementation Details

### A.1. finetuning details

Table 4. Hyperparameters for DIVER fine-tuning.

Hyperparameters	Settings
Epochs	50
Batch size	64
Dropout	0.1
Optimizer	AdamW
Learning rate	1e-4
Adam $\beta$	(0.9, 0.999)
Adam $\epsilon$	1e-8
Weight decay	5e-2
Scheduler	CosineAnnealingLR
Cosine cycle epochs	50
Minimal learning rate	1e-6
Clipping gradient norm	1
Label smoothing (multi-class classification)	0.1

By default, we used the same hyperparameters (Table 4) as CBraMod (Wang et al., 2024b) in component ablation analysis (Table 2) and channel permutation (Table 3) studies. Some of the cases in component analysis and channel permutation analysis did not show convergence, due to high learning rate. Trials that didn’t converge are listed below.

- w/o patch-wise CNN encoding with random seed 42
- w/o sepctral embedding with random seed 44
- w/o binary attention bias with random seed 44 in pretrain permute and finetuning naive condition

Learning rate was set as 5e-5 only for these trials to keep the consistency of using same random seeds of 41, 42, 43, 44, 45 for all other studies while following reported finetuning settings of CBraMod (Wang et al., 2024b).

## B. Reproducibility Problems in (Wang et al., 2024b)

Table 5. The results of different methods on downstream tasks tested on our setting

Methods	FACED, 9-class			PhsyioNet-MI, 4-class		
	Bal. Acc.(%)	Kappa(%)	F1(%)	Bal. Acc.(%)	Kappa(%)	F1(%)
EEGNet	16.3 $\pm$ 2.9	6.0 $\pm$ 3.4	10.6 $\pm$ 3.0	57.4 $\pm$ 0.8	43.2 $\pm$ 1.1	57.3 $\pm$ 0.8
SPaRCNet	15.3 $\pm$ 0.6	4.9 $\pm$ 0.7	9.6 $\pm$ 1.2	56.8 $\pm$ 0.7	42.4 $\pm$ 1.0	56.7 $\pm$ 0.9
ST-Transformer	21.9 $\pm$ 0.6	12.1 $\pm$ 0.7	21.0 $\pm$ 0.7	59.5 $\pm$ 0.8	45.9 $\pm$ 1.1	59.2 $\pm$ 0.9
EEGConformer	45.1 $\pm$ 1.2	37.9 $\pm$ 1.4	45.2 $\pm$ 1.3	57.4 $\pm$ 0.5	43.2 $\pm$ 0.6	57.4 $\pm$ 0.4
LaBraM-Base	46.6 $\pm$ 1.1	39.6 $\pm$ 1.2	46.4 $\pm$ 1.1	64.7 $\pm$ 0.7	52.9 $\pm$ 0.9	64.8 $\pm$ 0.8
CBraMod 10%	56.5 $\pm$ 0.8	51.0 $\pm$ 1.0	56.9 $\pm$ 0.8	62.4 $\pm$ 0.6	49.9 $\pm$ 0.8	62.6 $\pm$ 0.7
CBraMod	56.6 $\pm$ 1.2	50.9 $\pm$ 1.3	56.8 $\pm$ 1.2	61.2 $\pm$ 0.8	48.4 $\pm$ 1.0	61.4 $\pm$ 0.8

In order to compare and evaluate our results with previous studies, we tried to reproduce the performance of prior models. Table 6 shows performance of downstream tasks reported in CBraMod and Table 5 shows results of testing on our setting. Though we used the codes and model weights of the previous work, we were unable to replicate the reported results. Learning rate and weight decay used for the downstream task in previous baseline test are not disclosed. Due to these limitations, we cannot exactly yield the reported results. This might arise due to the selection of random seeds, which were

Table 6. Reported performance of downstream EEG tasks in CBraMod

<b>Methods</b>	<b>FACED, 9-class</b>			<b>PhsyioNet-MI, 4-class</b>		
	<b>Bal. Acc.(%)</b>	<b>Kappa(%)</b>	<b>F1(%)</b>	<b>Bal. Acc.(%)</b>	<b>Kappa(%)</b>	<b>F1(%)</b>
EEGNet	40.9 $\pm$ 1.2	33.4 $\pm$ 2.5	41.2 $\pm$ 1.4	58.1 $\pm$ 1.3	44.7 $\pm$ 2.0	58.0 $\pm$ 1.2
SPaRCNet	46.7 $\pm$ 1.6	39.8 $\pm$ 2.9	47.3 $\pm$ 1.3	59.3 $\pm$ 1.5	45.6 $\pm$ 2.3	59.4 $\pm$ 1.5
ST-Transformer	48.1 $\pm$ 0.8	41.4 $\pm$ 1.3	48.0 $\pm$ 1.0	60.4 $\pm$ 0.8	47.1 $\pm$ 2.0	60.5 $\pm$ 0.8
EEGConformer	45.6 $\pm$ 1.3	38.6 $\pm$ 1.9	45.1 $\pm$ 1.1	60.5 $\pm$ 1.0	47.4 $\pm$ 1.7	60.6 $\pm$ 1.0
LaBraM-Base	52.7 $\pm$ 1.1	47.0 $\pm$ 1.9	52.9 $\pm$ 1.0	61.7 $\pm$ 1.2	49.1 $\pm$ 1.9	61.8 $\pm$ 1.4
CBraMod	55.1 $\pm$ 0.9	50.4 $\pm$ 1.2	56.2 $\pm$ 0.9	64.2 $\pm$ 0.9	52.2 $\pm$ 1.7	64.3 $\pm$ 1.0

also not disclosed by authors. We utilized the identical code provided in github, ranging from preprocessing, pretraining and finetuning. Even when using opened pretrained weight from CBraMod produced results outside standard deviation for PhysioNet-MI while FACED resulted in a slightly better performance.